Sarcomere Alignment is Regulated by Myocyte Shape

Mark-Anthony Bray, Sean P. Sheehy, and Kevin Kit Parker*

Disease Biophysics Group, School of Engineering and Applied Sciences, Harvard University, Cambridge, Massachusetts

Cardiac organogenesis and pathogenesis are both characterized by changes in myocyte shape, cytoskeletal architecture, and the extracellular matrix (ECM). However, the mechanisms by which the ECM influences myocyte shape and myofibrillar patterning are unknown. We hypothesized that geometric cues in the ECM align sarcomeres by directing the actin network orientation. To test our hypothesis, we cultured neonatal rat ventricular myocytes on islands of micropatterned ECM to measure how they remodeled their cytoskeleton in response to extracellular cues. Myocytes spread and assumed the shape of circular and rectangular islands and reorganized their cytoskeletons and myofibrillar arrays with respect to the ECM boundary conditions. Circular myocytes did not assemble predictable actin networks nor organized sarcomere arrays. In contrast, myocytes cultured on rectangular ECM patterns with aspect ratios ranging from 1:1 to 7:1 aligned their sarcomeres in predictable and repeatable patterns based on highly localized focal adhesion complexes. Examination of averaged α-actinin images revealed invariant sarcomeric registration irrespective of myocyte aspect ratio. Since the sarcomere sub-units possess a fixed length, this observation indicates that cytoskeleton configuration is length-limited by the extracellular boundary conditions. These results indicate that modification of the extracellular microenvironment induces dynamic reconfiguring of the myocyte shape and intracellular architecture. Furthermore, geometric boundaries such as corners induce localized myofibrillar anisotropy that becomes global as the myocyte aspect ratio increases. Cell Motil. Cytoskeleton 65: 641–651, 2008. © 2008 Wiley-Liss, Inc.

INTRODUCTION

Altered myocyte shape is a hallmark of the normal maturation of the heart, as well as its response to pathological conditions. Of particular importance are the morphological changes induced in the ventricles by mechanical and hemodynamic stimuli that result in physiological or maladaptive hypertrophic responses at the cellular level. For the cylindrically-shaped myocyte, these changes are predominantly reflected in the ratio of the cell length to its width. The hypertrophic response associated with athletic training (i.e., physiological hypertrophy) is characterized by a proportional increase of both the myocyte length and width. The response to eccentric cardiomyopathy, however, leads to sarcomere assembly in series, producing a greater increase in the myocyte

*Correspondence to: Kevin Kit Parker, School of Applied Science and Engineering, Harvard University, 29 Oxford Street, 322A Pierce Hall, Cambridge, MA 02138, USA. E-mail: kkparker@seas.harvard.edu

length as compared to the width [Anversa et al., 1983; Gerdes et al., 1988]. In contrast, during concentric cardiomyopathy, the sarcomeres are assembled in parallel, resulting in an increase in myocyte width [Smith and Bishop, 1985; Anversa et al., 1986].

Alterations in myocyte morphology during heart disease appear to be associated with downstream changes in myocardial contractility. The length-to-width ratio of a normal myocyte decreases from a normal value of seven as a result of an increased myocyte width during pressure-overload hypertrophy as shown by Onodera et al [Onodera et al., 1998]. Myocyte lengthening through sarcomerogenesis produces in an increase in the diameter of the ventricular chamber but the absence of accompanying transverse growth results in a net thinning of the ventricular wall, which has been hypothesized by Gerdes et al to reduce the ventricular force output and ejection fraction [Gerdes and Capasso, 1995]. A similar effect has been observed in the left ventricle after myocardial infarction, in which dispersion in myocyte morphology contributed to an overall loss of cellular contractility [Capasso and Anversa, 1992]. Regardless of the etiology, adaptive and dynamic reorganization of the contractile machinery is concomitant with either normal or pathological myocyte remodeling and, in the maladaptive case, is associated with compromised mechanical performance.

The extracellular matrix (ECM) plays a crucial role in governing the morphological response of a myocyte to external perturbation. The physical coupling of the myocyte to the ECM is mediated by transmembrane receptors such as integrins, which further serve to transmit external mechanical forces into the intracellular space [Ingber, 1991; Brancaccio et al., 2006]. Sarcomeres, among other cytoskeletal structures, are capable of utilizing these mechanical signals to direct their assembly and growth [Simpson et al., 1999]. Interestingly, actin stress fiber formation subsequently follows the direction of external tension imposed on myocytes in vitro; the myocytes recruit focal adhesion complexes (FACs) to regions of high stress and these FACs are in turn connected to newly polymerized actin microfilaments [Torsoni et al., 2003]. These mechanical forces can be transduced into biochemical signals capable of altering protein synthesis and gene transcription [Maxwell and Hendzel, 2001], and indeed pathological cardiac hypertrophy provokes reexpression of fetal-type genes ordinarily inactive in the adult heart [Komuro and Yazaki, 1993] in addition to sarcomeric reassembly. Conversely, contractile forces intrinsically generated by the myocytes are transmitted to the surrounding ECM via costameres, structures physically coupling the sarcolemmal membrane to the peripheral Z-lines [Samarel, 2006]. However, the mechanisms by which the ECM and the subsequent alterations in the geometry influence myofibrillar patterning of the cardiac myocyte have yet to be elucidated.

While the impact of the ECM on cell morphology has been recognized for decades [Weiss and Garber, 1952], the recent development of techniques to control ECM deposition has created new avenues of research previously unavailable. Custom-designed microcontact printing (μCP) of ECM substrata offers precise control of adherent cell shape and size independent of cell-cell interaction and culture density [Singhvi et al., 1994]. The application of this technique to single fibroblast and endothelial cells has been used extensively to reveal details of the relationship between cellular function and morphology, e.g., cell spreading and adhesion formation [Lehnert et al., 2004], cell cycle progression [Huang et al., 1998], growth and apoptosis[Chen et al., 1997], and lamelopodia extension and cell migration [Parker et al., 2002]. However, similar studies of single cardiac myocytes has been more limited, especially in light of their higher contractility and distinct architecture as compared to non-muscle cells [Lin et al., 1989; Lu et al., 1992] Systematic alteration of the ECM microenvironment has been primarily concerned with tissue-level electrophysiology [Rohr et al., 1991; Bursac et al., 2004] and the response to mechanical stretch [Simpson et al., 1999; Gopalan et al., 2003; Beauchamp et al., 2006]. In this study, we hypothesized that spatial cues in the ECM promote sarcomere alignment by changing the myocyte shape and hence directing the orientation of the myofibrillar network. To test this hypothesis, we used μCP to create ECM islands to alter the geometric boundary conditions imposed on cultured cardiac myocytes, and systemically examined the morphological response as a function of myocyte shape by characterizing the organization of both the sarcomeric proteins and focal adhesion proteins. We quantified cytoskeletal architecture, including myofibrillar and sarcomeric alignment, with respect to myocyte shape. Our data demonstrate that cardiac myocytes will architecturally remodel and reassemble and reorganize their contractile cytoskeleton in response to geometric cues in the ECM. These findings comprise a step towards understanding the role of myocyte shape in cardiac myofibrillogenesis and its role in heart failure.

MATERIALS AND METHODS

The experimental protocols and data analysis methodology is described briefly here. Additional details are available as online Supplemental Material.

Experimental Protocol

Microcontact Printing and Cell Culture. Polymer stamps designed for microcontact printing were made with standard soft photolithographic techniques [Chen et al., 1998; Xia and Whitesides, 1998]. Silicon

wafers spin coated with a 2 μm layer of SU-8 photoresist (MichroChem Corp, Newton, MA) were exposed to UV light through a photolithographic mask, photodegrading SU-8 and leaving a complementary master pattern. μCP designs consisting of circles 26 μm in radius (2123.7 μm^2 area) and rectangular shapes with a constant surface area of 2500 μm^2 were used to create the ECM islands. Since studies have reported a range of myocyte length-to-width changes in diseased hearts, a variety of aspect ratios were created for the rectangular shapes: 1:1 (50 × 50 μm), 2:1 (70.7 × 35.4 μm), 3:1 (86.6 × 28.9 μm), 5:1 (111.8 × 22.3 μm) and 7:1 (132.3 × 18.9 μm).

Stamps were formed by pouring un-polymerized poly(dimethylsiloxane) (PDMS, Sylgard 184, Dow Corning, Midland, MI) over the master. The cured polymer was peeled off forming a complimentary 'stamp' of the surface. Glass coverslips spin-coated with a layer of PDMS were treated in a UVO cleaner (Jelight Company, Inc., Irvine, CA) prior to microcontact printing to oxidize the PDMS layer and facilitate the adsorption of ECM proteins onto the stamp. The protein fibronectin (FN) was chosen for μCP deposition for its efficacy in promoting myocyte spreading by activation of signaling pathways through β1 integrins [Hilenski et al., 1992]. The PDMS stamps were coated with 300 μL of a 50 μg/mL solution of FN for 1 h at room temperature, after which the patterned FN is manually stamped onto the coverslips. The portions of the coverslips not coated with FN were then blocked by immersing them in 1% F127 Pluronic Acid (BASF, Mount Olive, NJ) for 5 min in order to restrict cell adhesion to the FN islands. All stamped coverslips were washed in PBS and then seeded with neonatal rat ventricular myocytes prepared from two-day old Sprague-Dawley rats. Verification of our isolation protocol showed 92% of the cells recovered from excised tissue were cardiomyocytes. In order to prevent cell crowding on the isolated ECM islands, the myocyte seeding density was limited to 5×10^4 cells/coverslip. All animals were treated according to the guidelines published by the US National Institutes of Health.

Cell Fixation and Labeling. The myocytes were cultured for 4 days to insure full functional and morphological maturity based on observation of myocyte spreading upon the ECM island and myofibril development. Myocytes were fixed in a solution consisting of 4% paraformaldehyde and 0.01% Triton X-100 in PBS buffer at 37°C for 15 min and equilibrated to room temperature during incubation. All myocytes were stained with DAPI for chromatin and FITC-phalloidin for F-actin (Alexa 488 Phalloidin, Molecular Probes, Eugene, OR). The myocytes were also incubated with either mouse-derived IgG1 monoclonal primary sarcomeric anti-α-actinin (clone EA-53; Sigma-Aldrich, St. Louis, MO) or vinculin (clone hVIN-1; Sigma-Aldrich) antibodies at a dilution of 1:200 and incubated for 1 h in PBS. The myocytes were then incubated for 1 h with secondary antibody tetramethylrhodamine-conjugated goat anti-mouse IgG (Alexa Fluor 594, Molecular Probes) at a dilution of 1:200. All cells used for image analysis were verified to be cardiomyocytes by positive labeling of the Z-discs for sarcomeric α-actinin or the presence of striations in the actin immunofluorescence images.

Image Acquisition. The patterned myocytes were visualized with a CCD camera (CoolSnap Photometrics, Roper Scientific Inc., Trenton, NJ) mounted on an inverted microscope (DMI 6000B, Leica Microsystems, Germany). A 63× objective (HCX Plan APO, NA 1.4, Leica) was used for optical recording. The fluorescence recording was performed with a filter set with a bandpass excitation filter (450–490 nm), dichroic mirror (500 nm) and a bandpass emission filter (500–550 nm). Fluorescence was recorded in a format of 1392 × 1040 pixels (corresponding to 142.68 × 106.60 μm^2).

Data Analysis

Myocyte Geometric Registration and Averaging. Image data was taken only from those μCP ECM islands containing a single, mono-nucleated myocyte. Because of the inter-myocyte variation of parameters for a given shape, the data was transformed to a uniform coordinate system for image processing and analysis. Due to symmetry considerations, the location of the nuclear centroid was chosen as the fiducial marker to register each image, obtained from the DAPI fluorescence image via thresholding. Each shape was then registered by transformation to a uniform coordinate system with a unit radius (circles) or a normalized axis length based on the pre-defined myocyte aspect ratio (rectangles). Once each image was normalized and registered, an averaged F-actin and sarcomeric α-actinin image was obtained for each geometric shape by using top-hat filtering to remove non-uniform background fluorescence and then calculating the average pixel intensity over all myocyte images for a given shape.

Determination of Actin Anisotropy and Sarcomere Statistics. In addition to the myofibrillar density distribution given by the averaged image, the anisotropy of the myofibril network was computed from the normalized and registered immunofluorescence actin images to provide a measure of myofibril orientation. Each image was pre-processed using a modified ridge detection algorithm [Hong et al., 1998; Kovesi, 2005] to produce spatial maps of the myofibrils and the local orientation angle with respect to the y-axis. The angular statistics of these values was taken as a measure of the global anisotropy of the actin fibers (see ''Statistical Analysis''); if the myofibrils are parallel to the y-axis, the orientation angles will have a low angular spread (i.e., standard

error) and high anisotropy, whereas an isotropic set of myofibrils will have a higher angular spread and low anisotropy. The regularly-striated sarcomere structure was characterized in sarcomeric α-actinin images using a fast Fourier transform (FFT) to quantitatively calculate the local spatial frequencies. An intensity profile was chosen along lines towards the periphery of the myocyte parallel to the rectangular long axis, which was then detrended and weighted with a Hamming window prior to transformation into the spatial frequency domain by FFT. The spatial frequency at peak power of the first-order harmonic in the spatial frequency domain was obtained and converted into the spatial domain to yield the sarcomere length.

Statistical Analysis. All measurements are given as mean ± SEM. The circular mean and SEM (in degrees) were evaluated according to an angular distribution, and the cellular myofibril anisotropy was taken as 90°-SEM. Statistical significance was determined using one-way ANOVA, followed by Scheffé's multiple comparison test to determine differences. $P < 0.05$ was considered significant.

RESULTS

In all patterned and unpatterned myocyte cultures, spontaneously beating myocytes developed well-defined and differentiated myofibrils distributed throughout the cytoplasm after 96 h. Myocytes were characterized by the presence of periodically repeating I-bands highlighted by the phalloidin immunofluorescence, with the Z-lines revealed by the sarcomeric α-actinin stains. Whenever the myocytes attached to the ECM, whether the substrate was in the form of an island or an expanse of homogeneous ECM with no local boundary, they assembled vinculin-containing FAs and subsequently formed myofibrils with the terminal ends located on a vinculin plaque. Myofibrils crossing the medial region of the myocyte to terminate on a FA had no sarcomeres in the vicinity of the adhesion plaque, as revealed by the α-actinin stains.

Myofibrillogenesis in Unbounded Myocytes

Myocytes cultured on substrates with covered with uniform ECM were usually pleomorphic and characterized by generally isotropic cytoskeletal organization (Fig. 1). Such morphology is consistent with the absence of boundary conditions, resulting in myocytes of varying shape and size. These pleomorphic myocytes often possessed extensions of varied number, shape, and length (Figs. 1A and 1C).

The sarcomeric organization of the pleomorphic myocytes reflected the myofibrillar orientation: Z-lines were spatially registered in parallel in locally, i.e., sub-

cellular domains, especially in the vicinity of acute angles in the membrane boundary. Myofibrils in neighboring domains, however, were often aligned along different axes, indicating a lack of global anisotropy (Fig. 1B). The FAs revealed by vinculin were often restricted to the periphery of the myocyte. In many myocytes, vinculin manifested as a punctate pattern co-localized to the myofibril Z-discs, indicating the formation of costameres [Danowski et al., 1992]. For those myocytes with elongated extensions, the FAs were significantly larger in size and possessed a radiating pattern directed inwards from the terminus of the pointed extension towards the myocyte center (Fig. 1D).

Myofibrillogenesis in Circular Myocytes

The myofibrillar organization associated with myocytes cultured on circular ECM islands possessed no readily discernable pattern over the experimental duration. The FAs reflected this myofibril arrangement by the accumulation of vinculin on the myocyte circumference and distributed as punctuated foci radiating a short distance into the myocyte interior (Fig. 2B). Not all myofibrils spanned the full diameter of the myocyte; many of the myofibrils formed a shorter chord connecting two points on the myocyte circumference. Furthermore, myofibrils often did not form a straight filament spanning distal points on the myocyte but instead arced laterally across the diameter, sometimes bending around the perinuclear region (Fig. 2C). This heterogeneous myofibrillar distribution was apparent in the averaged actin images, in which no pattern is readily discernable (Fig. 2E). The average actin density is significantly lower towards the center of the myocyte; this void coincides with the distribution of the nuclei in the circular myocytes, thereby reflecting the displacement of the myofibrils around the nucleus. In accordance with the irregular myofibril arrangement, the Z-disc distribution in circular myocytes is similarly disorganized (Figs. 2D and 2F).

Myofibrillogenesis in Myocytes of Increasing Aspect Ratio

In contrast to the circular myocytes, the myocytes cultured on rectangular islands displayed a myofibrillar arrangement that was consistent for individual myocytes within each aspect ratio (AR) examined. Myofibrils in 1:1 AR (square) myocytes were found to radiate towards the corners of the myocyte, either paralleling the edge, or spanning the myocyte diagonally, to terminate at the corners. This myofibril organization was reflected in the vinculin distribution for square myocytes, accumulating as elongated plaques in a fan-shaped ensemble where the myofibrils terminated (Fig. 3Aii). Accordingly, the
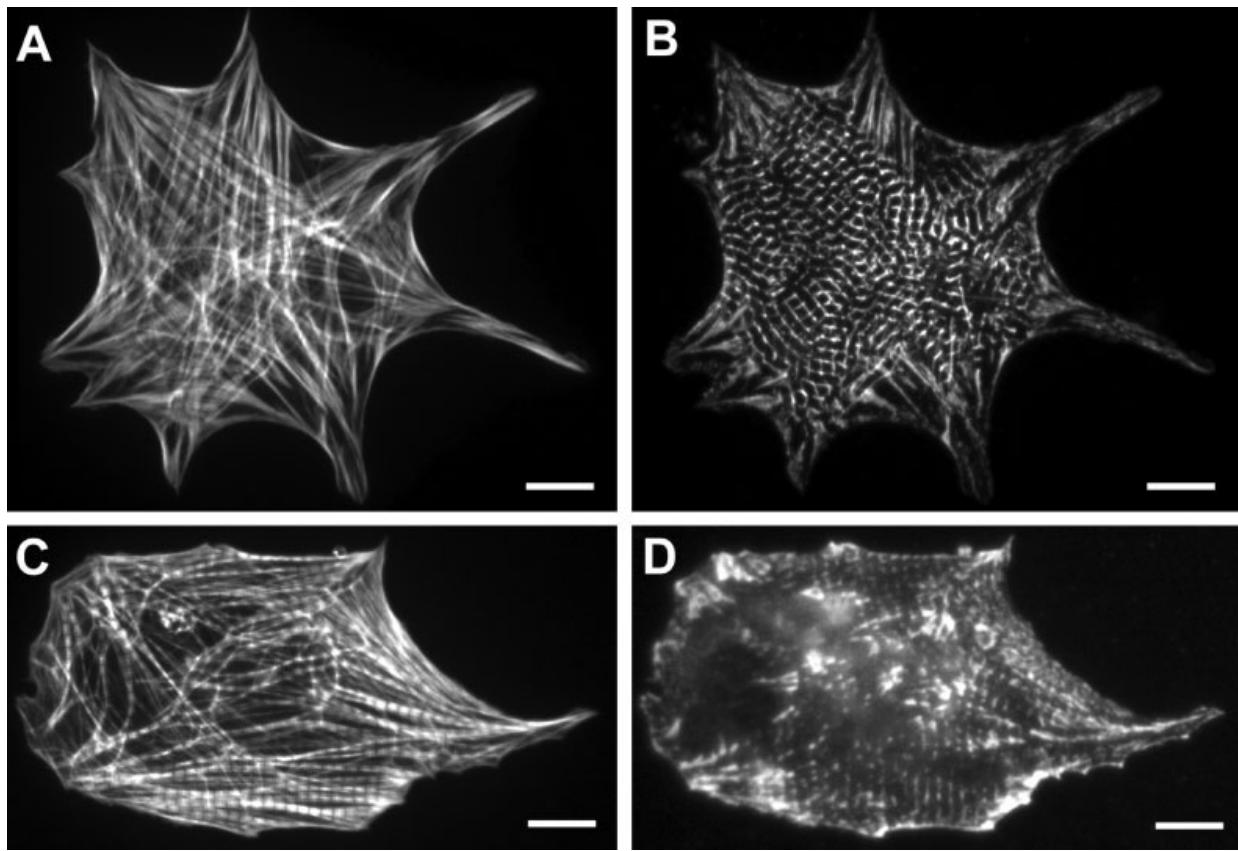
Fig. 1.   Distribution of actin (**A,C**) α-actinin (**B**) and vinculin (**D**) in pleomorphic cultured myocytes. One example myocyte is shown in (A) and (B), a different myocyte is shown in (C) and (D). Note the lack of myofibrillar and sarcomeric organization and multiple myofibril axes for both myocytes shown. Scale bar: 10 μm.

averaged actin distribution showed a similar pattern, as myofibrils from the medial region of the myocyte terminate on the FAs in the corners, they converged into a progressively narrower space. Similarly, while the myofibrils paralleled both the myocyte edges and diagonals (Fig. 3Aiii), the consistent spatial confinement of the actin along the edges produced a high myofibril density in those regions (Fig. 3Av).

As myocyte AR was increased, the myofibril and FA configurations changed accordingly, as shown in Figs. 3B and 3C and Figs. 4A and 4B. The FAs for the 2:1 myocytes were primarily restricted to the corners and maintained their fan-shaped morphology as in the square myocytes but the radiating pattern of the plaques were preferentially oriented parallel to the long axis of the myocytes (Fig. 3Bii). Similarly, the averaged actin distribution for the 2:1 myocytes revealed that while the myofibrils continued to locate their termini in the corners of the myocyte, the myofibrils generally paralleled the long axis of the myocyte, with less on the short edge or the diagonal (Fig. 3Biii). This trend continued for the 3:1, 5:1

and 7:1 rectangular myocytes, with the branches of the FAs of the 7:1 rectangular myocytes aligned strictly parallel to the long cellular axis (Fig. 4Bii). Likewise, the myofibrils were also restricted to the long axis with very few along the diagonal to the opposing corner and virtually none branching the short distance to the adjacent corner on the short axis of the myocyte (Fig. 4Biii). In addition, the averaged actin map indicates myofibrils located along the long axis of the myocyte were primarily located towards the edges, with the interior of the myocyte possessing a reduced density distribution of myofibrils. It should be pointed out that this edge effect is seemingly exacerbated by the displacement of myofibrils by the nucleus, usually located at the myocyte center. Since the averaged actin maps depict the myofibril density as opposed to their alignment, an anisotropy value was calculated to quantify the overall actin orientation for each myocyte shape (see ''Methods''). As shown in Fig. 4C, the square and circular myocytes possess comparably low anisotropy. However, as the AR for the rectangular myocytes increases, the myofibrillar
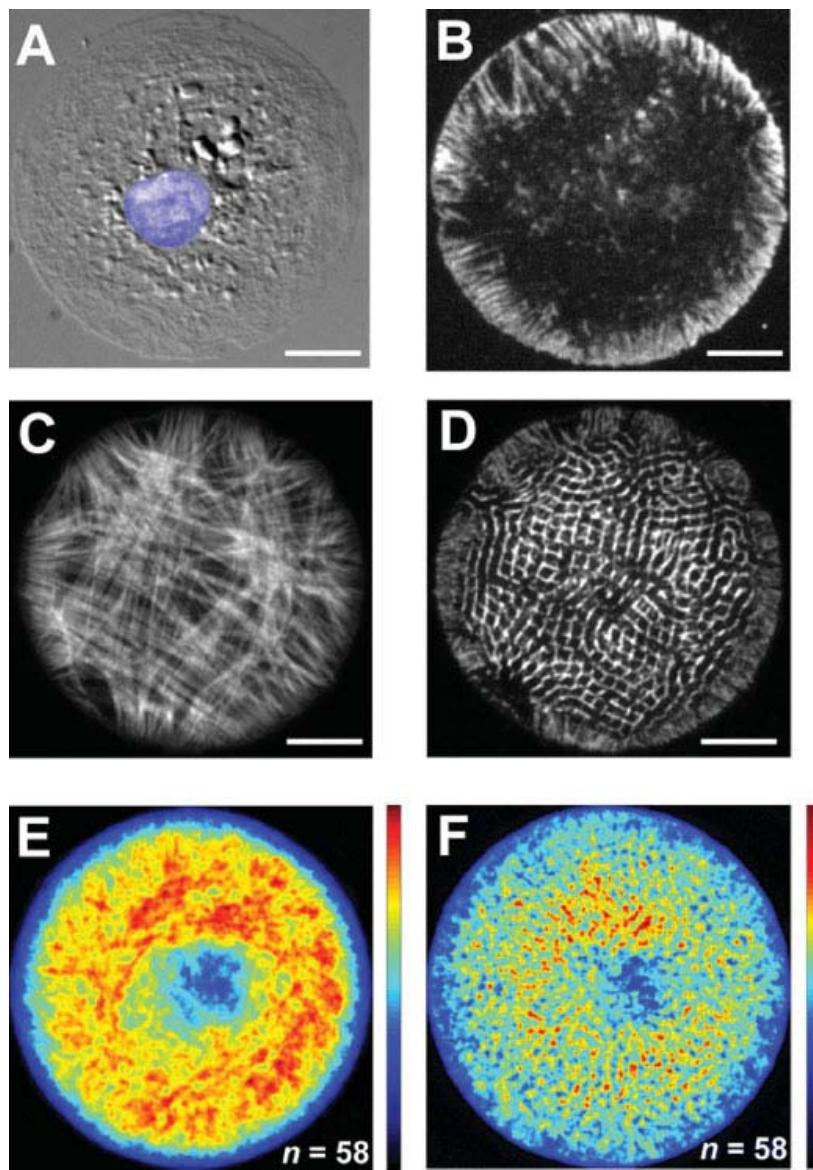
Fig. 2. (**A**) A DIC image of a cultured myocyte on a microcontact printed circular ECM island (radius: 26 μm) with the nucleus colored in blue. (**B**) FAs linking the myocyte to the ECM are highlighted by stained vinculin. The associated F-actin (**C**) and sarcomeric α-actinin (**D**) in a representative circular myocyte shows the absence of a preferential axis of organization. The resultant sarcomere organization for an ensemble of circular myocytes is illustrated via averaged images of F-actin (**E**) and sarcomeric α-actinin (**F**) distributions from fixed and stained myocytes. Scale bars: 10 μm.

anisotropy concomitantly increases as the myofibrils become more parallel.

Sarcomere Alignment in Rectangular Myocytes

The averaged distribution maps of α-actinin permitted quantification at the sarcomere level of the myocyte response to the ECM boundaries. For the square myocytes, the myofibril orientation towards the myocyte corners produced a characteristic moiré pattern in the averaged α-actinin distribution map (Fig. 5A). As the AR was increased, the change in the myofibrillar arrangement from radial to longitudinal resulted in Z-line orientations increasingly oriented perpendicular to the long axis of the myocyte (Fig. 5A). As the myofibrils approached the terminal FAs, the striations often termi-

nated abruptly into non-striated areas with punctuate α-actinin coincident with the adhesion plaques. The co-localization of α-actinin with FAs is consistent with previous observations [Hilenski et al., 1991].

Given the repeatability of myofibril distribution in the shaped myocytes, we turned to the question of whether the consistency in myofibril distribution due to μCP ECM shape also leads to predictable sarcomere positioning as well. Examining the averaged images of the sarcomeric α-actinin (Fig. 5A), it is immediately apparent that striations are visible in the distribution map. Since the distribution map for each AR is the cumulative average of an ensemble of myocytes, it was anticipated that the cell-to-cell variation in Z-disc placement would result in a more uniform intensity distribu-
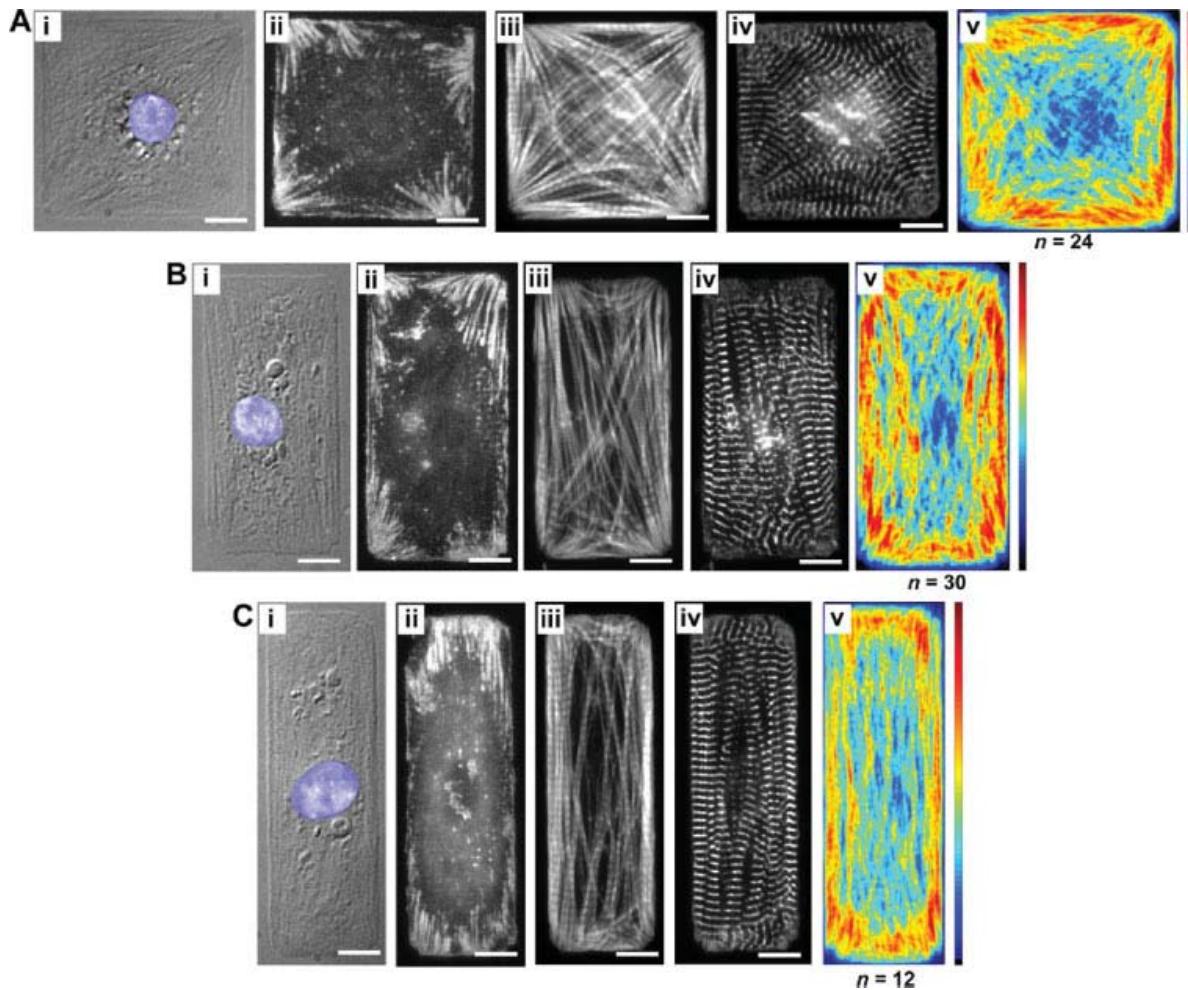
Fig. 3. Cardiac myocytes on rectangular microcontact printed (μCP) ECM islands, FAs highlighting the myocyte-ECM contacts, and cytoskeletal architecture and averaged myofibrillar organization. Three cellular aspect ratios are shown: (A) 1:1, (B) 2:1, and (C) 3:1. A DIC image and immunofluorescent stains for vinculin, F-actin and sarcomeric α-actinin of a representative cardiac myocyte on a μCP ECM island are shown in panels (i)–(iv), respectively. The averaged distribution of F-actin for each cellular aspect ratio is shown in panel (v).

tion. Therefore, the observation of distinct striations even with averaging of the α-actinin fluorescence was an unexpected result. On this basis, we posit that the sarcomeres were spatially registered along the myofibril for myocytes of a given length. Therefore, the striations are consistent in the averaged α-actinin distribution despite heterogeneities between myocytes of a given AR. To test whether the periodicity was an artifact of the average distribution map or reflected the underlying sarcomere structure, the spatial frequency was determined from the profiles using the FFT procedure described in the Methods section. Graphs of intensity profiles chosen close to the myocyte edge and along the myocyte length are shown in Fig. 5B for each AR, each of which exhibits a periodic structure. The results from determining the

dominant frequency are given in Table I. All of these measurements fall near the typical range for sarcomere length reported in cultured myocytes (1.94–2.1 μm) [Mansour et al., 2004]. The regular positioning of the sarcomeres within a given AR group suggests that the contractile architecture is tightly regulated by complex control measures, for example the interaction of the intracellular boundary conditions such as the internal angles of the rectangular myocyte and the positioning of the nucleus.

DISCUSSION

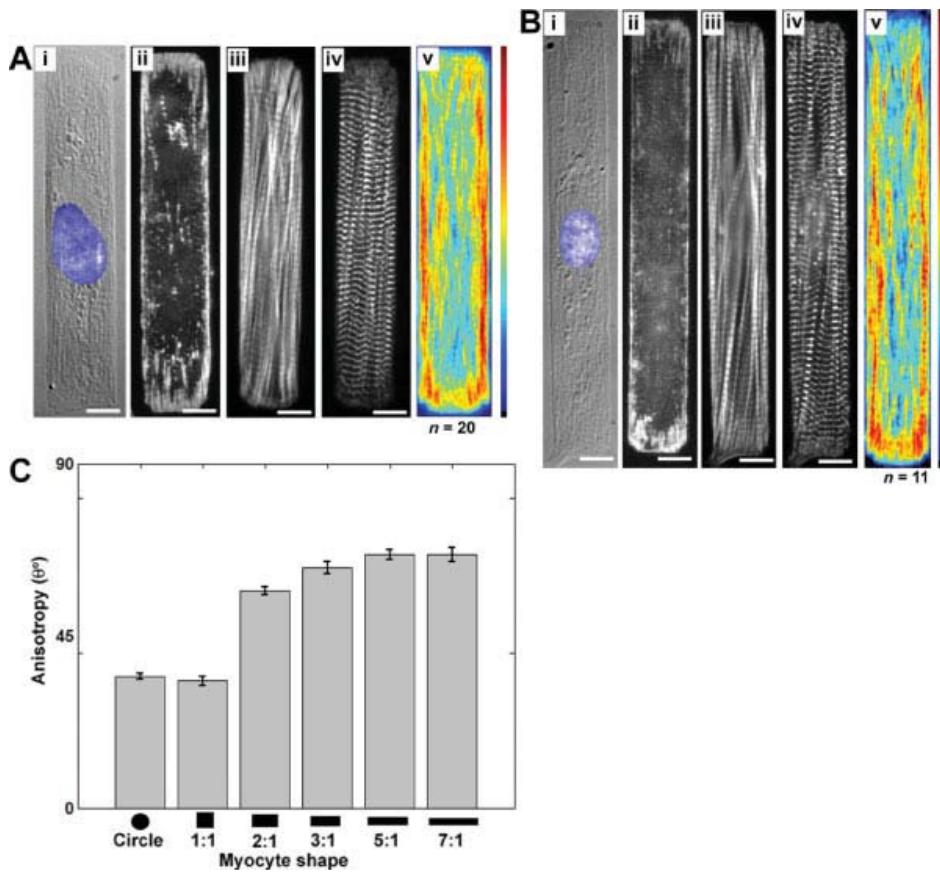The role of the ECM and cell shape as a signaling mechanism for cardiac myocytes has important implica-

Fig. 4. Cardiac myocytes on rectangular microcontact printed (µCP) ECM islands, FAs highlighting the myocyte-ECM contacts, and cytoskeletal architecture and averaged myofibrillar organization. Two cellular aspect ratios are shown: (A) 5:1 and (B) 7:1. A DIC image and immunofluorescent stains for vinculin, F-actin and sarcomeric α-actinin of a representative cardiac myocyte on a µCP ECM island are shown in panels (i)–(iv), respectively. The averaged distribution of F-actin for each cellular aspect ratio is shown in panel (v). (C) Anisotropy of the myofibrillar network as a function of the myocyte shape. Bars are given as mean ± SEM of the angular standard error of the actin cytoskeleton orientation. Statistically significant differences were found between the circular and 1:1 myocytes as compared to the remaining shapes, as well as between 2:1 myocytes and myocytes with AR > 5:1.

tions in for cardiac morpho- and patho-genesis, as well as the potential efficacy of therapeutic cell and tissue engineering. For example, our data suggest that functional heart grafts will require substrates that sufficiently recapitulate the extracellular microenvironment to ensure proper contractility and electrical function [Furuta et al., 2006]. Similarly, the ECM provides structural integrity and support for the heart at the cellular and organ levels, and alterations in fibrillar collagen distribution and geometry (e.g., stiffness induced by fibrosis) have been linked to diastolic dysfunction and heart failure [Brower et al., 2006]. In addition, disruption of the integrin linkages to the surrounding ECM may lead to cardiac myocytes detaching from their adhesion sites (anoikis) and
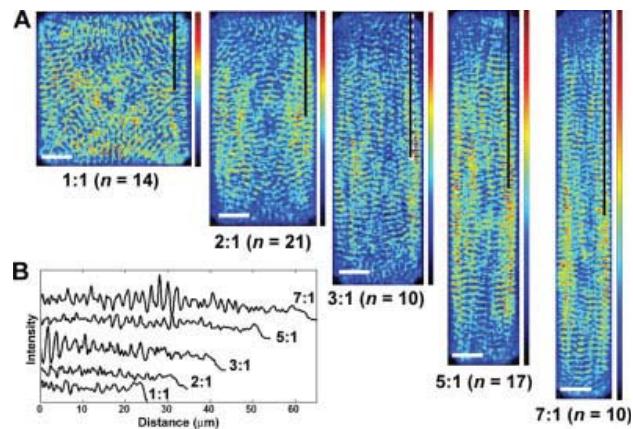

Fig. 5. (A) Average distribution of sarcomeric α-actinin from fixed and stained rectangular myocytes. Each myocyte was registered to a uniform coordinate system, normalized and the pixel intensity was averaged over all myocytes. Scale bar is 10 µm for all panels. (B) Intensity profiles from the averaged images as a function of distance along the black lines illustrated in (A). The lines are offset in the y-axis for clarity.

TABLE I. Sarcomere Length Estimated from Intensity Profiles Obtained from the Averaged Sarcomeric α-Actinin Images Shown in Fig. 5, for 1:1 ($n = 14$), 2:1 ($n = 21$), 3:1 ($n = 10$), 5:1 ($n = 17$), and 7:1 ($n = 10$)

Aspect ratio	Sarcomere length (µm)
1:1	2.27 ± 0.08
2:1	2.25 ± 0.11
3:1	1.98 ± 0.03
5:1	2.09 ± 0.05
7:1	1.96 ± 0.05

Values calculated by finding the dominant frequency present in the FFT of the intensity profiles. Values given as mean ± SEM. No statistically significant differences were found for $P < 0.01$.

has been proposed to contribute to apoptosis [Ding et al., 2000].

Myocytes cultured on circular islands were spatially confined by a well defined boundary, yet the resultant myofibrillar organization exhibited no consistent pattern. The radii of the ECM islands were sufficiently small to prevent spreading into pleomorphic shapes and permitted the formation of focal contacts guided by the ECM boundary (Fig. 2B). The thin, ring-like FA patterning of the circular myocytes was consistent with those reported for other cell types [O'Neill et al., 1990; Chen et al., 2003]. However, as seen in Figs. 2E and 2F, the absence of a repeatable cytoskeletal architecture for the circular myocytes demonstrated that the mere presence of a shape-restricting microenvironment is insufficient to govern sarcomerogenesis into the uniaxial contractile structure seen in vivo. The large variety in cytoskeletal organization observed for these circular myocytes, despite the consistent boundary conditions, is similar to prior studies where endothelial cells and fibroblasts cultured on circular ECM islands produced motility or lamellipodia formation in random directions [Parker et al., 2002; Jiang et al., 2005]. Thus it would appear that the myofibrillar self-assembly and organizational processes of the cell are optimized for unique extracellular cues.

The presence of unique geometric cues, such as corners, gave rise to persistent myofibrillar organizational patterns. Elongated vinculin-rich focal contacts in the corners oriented towards the myocyte center were a signature of myocytes with a lower AR (panels ii of Figs. 3A and 3B). The FA morphology for the square cardiac myocytes resembled those previously observed in square non-muscle cells [Parker et al., 2002; Chen et al., 2003]. Also, the same FA structure was noticeable in pleomorphic myocytes with elongated extensions; the narrow angle formed by the extension led to the formation of larger FAs than in myocytes with curved edges (Fig. 1D). Whether in vivo [Tokuyasu, 1989] or in vitro [Rothen-Rutishauser et al., 1998] it appears that myofibrillogenesis is preceded by the polymerization of actin fibers which are anchored to FAs that mature during sarcomerogenesis.

The reconfiguring of the FAs as the AR of the myocyte was increased appears coupled to the parallel bundling of the attached myofibrils. The myofibrillar arrangement of myocytes cultured on circular ECM islands was also observed with the actin stress fiber network in similarly patterned fibroblasts [O'Neill et al., 1990]. Likewise, fibroblasts on thin, linear ECM substrates produced tightly parallel bundles of stress fibers [O'Neill et al., 1990] in similar fashion to the myofibril orientation in rectangular myocytes with high AR. Hence, it is convenient to consider these two sets of boundary conditions as limiting examples of myofibrillar organization. Between these extremes, the myofibrils

underwent a transition in directional anisotropy: from alignment along multiple axes in the square myocytes (parallel to the four membrane edges and the two diagonals) towards alignment along a single axis in the 7:1 myocytes (Fig. 4C). Adult cardiac myocytes isolated from normal hearts have an AR of ∼7.5, while myocytes from hearts with concentric hypertrophy and dilated cardiomyopathy decrease and increase their ARs, respectively [Smith and Bishop, 1985; Gerdes et al., 1992]. Even so, a variety of diameters and lengths have been reported in the literature for myocytes isolated from diseased hearts [Shozawa et al., 1990; Beltrami et al., 1994; Scholz et al., 1994; del Monte et al., 1995]. While the cardiac ECM scaffold alone is sufficient to support a degree of cellular organization and functionality at the organ level [Ott et al., 2008], how the precise physical cues presented by the ECM influence cellular morphogenesis is still unclear. Therefore, culturing myocytes into a range of AR using μCP offers a promising in vitro experimental model of structural pathophysiology to examine and predict alterations in myofibril development concomitantly with cellular shape.

Mechanical stresses are transmitted between the cytoskeleton and the ECM via transmembrane integrin proteins which act to stabilize the FAs [Ezzell et al., 1997]. Studies quantifying the tractional forces of square non-muscle cells reveal significant tensile forces were exerted at the cell corners, whereas circular non-muscle cells do not produce a spatially consistent force profile [Parker et al., 2002; Wang et al., 2002]. Our results show that the FAs in rectangular myocytes promoted directed myofibril assembly and localized preferentially at the corners and ends of the myocyte. Therefore, it is expected that the maximal contractile forces for the rectangular cardiac myocytes will also be confined to regions where the myofibrils spatially converge, i.e., the corners of low AR myocytes and the ends of high AR myocytes. Such a result can be inferred from quantification of forces induced by contracting pleomorphic myocytes [Balaban et al., 2001]. If variations in myocyte shape are coupled to myocyte contractility as previously reported [Gerdes and Capasso, 1995], our data would suggest that the underlying cytoskeletal architecture may be the cause.

The arrangement of individual sarcomeres of mature myofibrils indicates a high level of spatial integration; sarcomeres are characterized by close apposition and lateral registry, and this arrangement is maintained by intermediate filaments connecting the Z-lines [Tokuyasu et al., 1985]. Conversely, deterioration of lateral sarcomeric registry has been shown be associated with suppressed contractility [Simpson et al., 1996] and exposure to stretch along the transverse cellular axis [Atherton et al., 1986]. For this study, we used averaged

α-actinin distribution maps to examine and quantify the degree of spatial alignment of the individual Z-lines and hence the sarcomeres. As seen in Fig. 5, the distribution maps indicate that sarcomere registration occurs not only longitudinally along a myofibril, but also transversely. The size of the vinculin-containing FA is proportional to the stress fiber length in non-muscle cells [Théry et al., 2006] and corresponds to the non-striated portion of the myofibril in cardiac myocytes [Hilenski et al., 1991]. Thus, the length of the non-striated portion should nominally be the same at both ends of a myofibril, and hence the striated portions should begin and terminate at roughly the same point across the cell length. This suggests that myofibrillogenesis proceeds in part based on the extracellular boundary configuration and the longitudinal assembly of the developing sarcomere is limited accordingly. The myofibril termini in our patterned myocytes were usually devoid of striations, typical for cardiac myocyte-ECM interfaces [Lu et al., 1992]. However, this is not the case for myocyte-myocyte connections at the intercalated lines, where Z-lines are associated with the adherens junction [Lu et al., 1992]. Therefore, the alignment of sarcomeres by a length-sensitive regulation of myofibrillogenesis may not be restricted to the single myocyte level but may also promote tissue-wide registration of the contractile machinery via the interconnectivity of the cardiac syncytium. Such a phenomenon has already been noted in cardiac tissue constructs patterned on aligned ECM substrates [Camelliti et al., 2005].

In summary, the reorganization of the cardiac myocyte myofibrillar structure in response to geometric cues encoded in the ECM leads to distinctive and predictable cytoskeletal architectures. As myocyte AR increases, spatial anisotropy, including aligned myofibrils and the registration of adjacent sarcomeres registration, emerges, suggesting that myocyte shape may be an important regulator of myocyte contractility. This hypothesis may reveal how changes in ECM during cardiomyopathies contribute to contractile dysfunction.

ACKNOWLEDGMENTS

REFERENCES

Anversa P, Levicky V, Beghi C, McDonald SL, Kikkawa Y. 1983. Morphometry of exercise-induced right ventricular hypertrophy in the rat. Circ Res 52:57–64.

Anversa P, Ricci R, Olivetti G. 1986. Quantitative structural analysis of the myocardium during physiologic growth and induced cardiac hypertrophy: a review. J Am Coll Cardiol 7:1140–1149.

Atherton BT, Meyer DM, Simpson DG. 1986. Assembly and remodelling of myofibrils and intercalated discs in cultured neonatal rat heart cells. J Cell Sci 86:233–248.

Balaban NQ, Schwarz US, Riveline D, Goichberg P, Tzur G, Sabanay I, Mahalu D, Safran S, Bershadsky A, Addadi L, Geiger B. 2001. Force and focal adhesion assembly: a close relationship studied using elastic micropatterned substrates. Nat Cell Biol 3:466–472.

Beauchamp P, Yamada KA, Baertschi AJ, Green K, Kanter EM, Saffitz JE, Kléber AG. 2006. Relative contributions of connexins 40 and 43 to atrial impulse propagation in synthetic strands of neonatal and fetal murine cardiomyocytes. Circ Res 99:1216–1224.

Beltrami CA, Finato N, Rocco M, Feruglio GA, Puricelli C, Cigola E, Quaini F, Sonnenblick EH, Olivetti G, Anversa P. 1994. Structural basis of end-stage failure in ischemic cardiomyopathy in humans. Circulation 89:151–163.

Brancaccio M, Hirsch E, Notte A, Selvetella G, Lembo G, Tarone G. 2006. Integrin signalling: the tug-of-war in heart hypertrophy. Cardiovasc Res 70:422–433.

Brower GL, Gardner JD, Forman MF, Murray DB, Voloshenyuk T, Levick SP, Janicki JS. 2006. The relationship between myocardial extracellular matrix remodeling and ventricular function. Eur J Cardiothorac Surg 30:604–610.

Bursac N, Aguel F, Tung L. 2004. Multiarm spirals in a two-dimensional cardiac substrate. Proc Natl Acad Sci USA 101:15530–15534.

Camelliti P, McCulloch AD, Kohl P. 2005. Microstructured cocultures of cardiac myocytes and fibroblasts: a two-dimensional in vitro model of cardiac tissue. Microsc Microanal 11:249–259.

Capasso JM, Anversa P. 1992 Mechanical performance of spared myocytes after myocardial infarction in rats: effects of captopril treatment. Am J Physiol Heart Circ Physiol 263:H841–H849.

Chen CS, Mrksich M, Huang S, Whitesides GM, Ingber DE. 1997. Geometric control of cell life and death. Science 276:1425–1428.

Chen CS, Mrksich M, Huang S, Whitesides GM, Ingber DE. 1998. Micropatterned surfaces for control of cell shape, position, and function. Biotechnol Prog 14:356–363.

Chen CS, Alonso JL, Ostuni E, Whitesides GM, Ingber DE. 2003. Cell shape provides global control of focal adhesion assembly. Biochem Biophys Res Commun 307:355–361.

Danowski BA, Imanaka-Yoshida K, Sanger JM, Sanger JW. 1992. Costameres are sites of force transmission to the substratum in adult rat cardiomyocytes. J Cell Biol 118:1411–1420.

del Monte F, O'Gara P, Poole-Wilson PA, Yacoub M, Harding SE. 1995. Cell geometry and contractile abnormalities of myocytes from failing human left ventricle. Cardiovasc Res 30:281–290.

Ding B, Price RL, Goldsmith EC, Borg TK, Yan X, Douglas PS, Weinberg EO, Bartunek J, Thielen T, Didenko V, Lorell BH. 2000. Left ventricular hypertrophy in ascending aortic stenosis mice: Anoikis and the progression to early failure. Circulation 101:2854–2862.

Ezzell RM, Goldmann WH, Wang N, Parasharama N, Ingber DE. 1997. Vinculin promotes cell spreading by mechanically coupling integrins to the cytoskeleton. Exp Cell Res 231:14–26.

Furuta A, Miyoshi S, Itabashi Y, Shimizu T, Kira S, Hayakawa K, Nishiyama N, Hagiwara Y, Satoh T, Fukuda K, Okano T, Ogawa S. 2006. Pulsatile cardiac tissue grafts using a novel

three-dimensional cell sheet manipulation technique functionally integrates with the host heart, in vivo. Circ Res 98:705–712.

Gerdes AM, Capasso JM. 1995. Structural remodeling and mechanical dysfunction of cardiac myocytes in heart failure. J Mol Cell Cardiol 27:849–856.

Gerdes AM, Campbell SE, Hilbelink DR. 1988. Structural remodeling of cardiac myocytes in rats with arteriovenous fistulas. Lab Invest 59:857–861.

Gerdes AM, Kellerman SE, Moore JA, Muffly KE, Clark LC, Reaves PY, Malec KB, McKeown PP, Schocken DD. 1992. Structural remodeling of cardiac myocytes in patients with ischemic cardiomyopathy. Circulation 86:426–430.

Gopalan SM, Flaim C, Bhatia SN, Hoshijima M, Knoell R, Chien KR, Omens JH, McCulloch AD. 2003. Anisotropic stretch-induced hypertrophy in neonatal ventricular myocytes micropatterned on deformable elastomers. Biotechnol Bioeng 81:578–587.

Hilenski LL, Terracio L, Borg TK. 1991. Myofibrillar and cytoskeletal assembly in neonatal rat cardiac myocytes cultured on laminin and collagen. Cell Tissue Res 264:577–587.

Hilenski LL, Ma XH, Vinson N, Terracio L, Borg TK. 1992. The role of β_1 integrin in spreading and myofibrillogenesis in neonatal rat cardiomyocytes in vitro. Cell Motil Cytoskeleton 21:87–100.

Hong L, Wan Y, Jain AK. 1998. Fingerprint image enhancement: algorithm and performance evaluation. IEEE Transactions on Pattern Analysis and Machine Intelligence 20:777–789.

Huang S, Chen CS, Ingber DE. 1998. Control of cyclin D1, p27(Kip1), and cell cycle progression in human capillary endothelial cells by cell shape and cytoskeletal tension. Mol Biol Cell 9:3179–3193.

Ingber D. 1991. Integrins as mechanochemical transducers. Curr Opin Cell Biol 3:841–848.

Jiang X, Bruzewicz DA, Wong AP, Piel M, Whitesides GM. 2005. Directing cell migration with asymmetric micropatterns. Proc Natl Acad Sci USA 102:975–978.

Komuro I, Yazaki Y. 1993. Control of cardiac gene expression by mechanical stress. Annu Rev Physiol 55:55–75.

Kovesi P. 2005. MATLAB and octave functions for computer vision and image processing. The University of Western Australia, The School of Computer Science and Software Engineering. [Accessed 3 October 2007; http://www.csse.uwa.edu.au/~pk/Research/MatlabFns/].

Lehnert D, Wehrle-Haller B, David C, Weiland U, Ballestrem C, Imhof BA, Bastmeyer M. 2004. Cell behaviour on micropatterned substrata: Limits of extracellular matrix geometry for spreading and adhesion. J Cell Sci 117:41–52.

Lin ZX, Holtzer S, Schutheiss T, Murray J, Masaki T, Fishman DA, Holtzer H. 1989. Polygons and adhesion plaques and the disassembly and assembly of myofibrils in cardiac myocytes. J Cell Biol 108:2355–2367.

Lu MH, DiLullo C, Schutheiss T, Holtzer S, Murray JM, Choi J, Fischman DA, Holtzer H. 1992. The vinculin/sarcomeric-alpha-actinin/alpha-actin nexus in cultured cardiac myocytes. J Cell Biol 117:1007–1022.

Mansour H, de Tombe PP, Samarel AM, Russell B. 2004. Restoration of resting sarcomere length after uniaxial static strain is regulated by protein kinase $C\varepsilon$ and focal adhesion kinase. Circ Res 94:642–649.

Maxwell CA, Hendzel MJ. 2001. The integration of tissue structure and nuclear function. Biochem Cell Biol 79:267–274.

O'Neill CO, Jordan P, Riddle P, Ireland G. 1990. Narrow linear strips of adhesive substratum are powerful inducers of both growth and total focal contact area. J Cell Sci 95:577–586.

Onodera T, Tamura T, Said S, McCune SA, Gerdes AM. 1998. Maladaptive remodeling of cardiac myocyte shape begins long before failure in hypertension. Hypertension 32:753–757.

Ott HC, Matthiesen TS, Goh S-K, Black LD, Kren SK, Netoff TI, Taylor DA. 2008. Perfusion-decellularized matrix: using nature's platform to engineer a bioartificial heart. Nat Med 14:213–221.

Parker KK, Brock AL, Brangwynne C, Mannix RJ, Wang N, Ostuni E, Geisse NA, Adams JC, Whitesides GM, Ingber DE. 2002. Directional control of lamellipodia extension by constraining cell shape and orienting cell tractional forces. FASEB J 16:1195–1204.

Rohr S, Scholly DM, Kléber AG. 1991. Patterned growth of neonatal rat heart cells in culture. Morphological and electrophysiological characterization. Circ Res 68:114–130.

Rothen-Rutishauser BM, Ehler E, Perriard E, Messerli JM, Perriard JC. 1998. Different behaviour of the non-sarcomeric cytoskeleton in neonatal and adult rat cardiomyocytes. J Mol Cell Cardiol 30:19–31.

Samarel AM. 2006. Costameres, focal adhesions, and cardiomyocyte mechanotransduction. Am J Physiol Heart Circ Physiol 289:H2291–H2301.

Scholz D, Diener W, Schaper J. 1994. Altered nucleus/cytoplasm relationship and degenerative structural changes in human dilated cardiomyopathy. Cardioscience 5:127–138.

Shozawa T, Okada E, Kawamura K, Sageshima M, Masuda H. 1990. Development of binucleated myocytes in normal and hypertrophied human hearts. Am J Cardiovasc Pathol 3:27–36.

Simpson DG, Sharp WW, Borg TK, Price RL, Terracio L, Samarel AM. 1996. Mechanical regulation of cardiac myocyte protein turnover and myofibrillar structure. Am J Physiol Cell Physiol 270:C1075–C1087.

Simpson DG, Majeski M, Borg TK, Terracio L. 1999. Regulation of cardiac myocyte protein turnover and myofibrillar structure in vitro by specific directions of stretch. Circ Res 85:e59–e69.

Singhvi R, Kumar A, Lopez GP, Stephanopoulos GN, Wang DI, Whitesides GM, Ingber DE. 1994. Engineering cell shape and function. Science 264:696–698.

Smith SH, Bishop SP. 1985. Regional myocyte size in compensated right ventricular hypertrophy in the ferret. J Mol Cell Cardiol 17:1005–1011.

Théry M, Pépin A, Dressaire E, Chen Y, Bornens M. 2006. Cell distribution of stress fibres in response to the geometry of the adhesive environment. Cell Motil Cytoskeleton 63:341–355.

Tokuyasu KT. 1989. Immunocytochemical studies of cardiac myofibrillogenesis in early chick embryos. III. Generation of fasciae adherentes and costameres. J Cell Biol 108:43–53.

Tokuyasu KT, Maher PA, Dutton AH, Singer SJ. 1985. Intermediate filaments in skeletal and cardiac muscle tissue in embryonic and adult chicken. Ann NY Acad Sci 455:200–212.

Torsoni AS, Constancio SS, Nadruz W, Jr., Hanks SK, Franchini KG. 2003. Focal adhesion kinase is activated and mediates the early hypertrophic response to stretch in cardiac myocytes. Circ Res 93:140.

Wang N, Ostumi E, Whitesides GM, Ingber DE. 2002. Micropatterning tractional forces in living cells. Cell Motil Cytoskeleton 52:97–106.

Weiss P, Garber B. 1952. Shape and movement of mesenchyme cells as functions of the physical structure of the medium: contributions to a quantitative morphology. Proc Natl Acad Sci USA 38:264–280.

Xia Y, Whitesides GM. 1998. Soft lithography. Ann Rev Mater Sci 28:153–184.